

Temporal dynamics of Lévy flights of photons in a hot vapor

R. V. M. de Almeida Filho,¹ J. C. de Aquino Carvalho,¹
T. Passerat de Silans,² M. H. G. de Miranda,¹ and M. O. Araújo^{1,*}

¹*Departamento de Física, Universidade Federal de Pernambuco, 50670-901, Recife, Pernambuco, Brazil*

²*Departamento de Física, CCEN, Universidade Federal da Paraíba,
Caixa Postal 5008, 58051-900, João Pessoa, Paraíba, Brazil*

(Dated: March 20, 2026)

Multiple scattering of light by resonant vapor is characterized by Lévy-type superdiffusion with a step size distribution $P(x) \propto 1/x^{1+\alpha}$, with $0 < \alpha < 2$. The Lévy parameter α was measured from $P(x)$, steady fluorescence, frequency-dependent fluorescence and time-resolved transmission, all of them in the forward direction. Here we report first measurements of this quantity from time-resolved backward fluorescence, i.e., photons that are backward diffused from light pulses exciting a hot rubidium vapor. We show experimentally that α can be extracted from this diffuse reflection, and the results are consistent with time-resolved transmission (i.e., photons that are forward diffused) and steady frequency-dependent forward fluorescence. Theoretical simulations are consistent with these results. We also show that, although we measure $\alpha = 1$ for both transmission and reflection, the backward photons have a non-negligible amount of single scattering events even for high density, contrary to the forward photons where multiple scattering dominates.

I. INTRODUCTION

Random walk of particles have applications in a large variety of systems, with the Brownian motion of particles the most known example. This motion is characterized by a random walk with successive jumps of size x , performed with finite step-size variance within a Gaussian distribution. However, in the last decades, random walks with diverging step-size variance were extensively studied, known as Lévy flights or Lévy walks. For this kind of random walk, the probability distribution for the step size x is given by $P(x) \propto 1/x^{\alpha+1}$, where $0 < \alpha < 2$ is the Lévy parameter. Lévy flights or walks are encountered in several kind of systems, ranging from animal foraging [1, 2], phonon transport in nanowires [3] and isolation of individuals between populations [4].

Light propagation in turbid media is often described by standard random walk and diffusion equations, like in biological tissues [5] and cold atoms [6]. However, in astrophysics [7], photonic materials dubbed Lévy glasses [8] and hot atomic vapors [9], Lévy flights can provide the correct statistical framework to describe superdiffusive transport of photons. In astrophysics and hot vapors, the Lévy statistics arises from multiple resonant scattering events and cannot be fully described by normal Brownian diffusion. In this process, photons are absorbed and re-emitted by the atoms with a different frequency which depends on the atomic velocity and collisions. Because of Doppler and eventual collisional broadening, the re-emitted photons have their frequencies non-correlated with the input frequency (i.e., complete frequency redistribution), which allows some photons to appear in the far spectral wings and they travel long distances before being reabsorbed [10–12]. These long and rare

flights produce a power-law step size distribution with $\alpha = 1$ ($\alpha = 0.5$) for non-collisional (collisional) broadening, defining the experimental signature of Lévy flights and superdiffusion. Modelling photon propagation in alkaline vapor as a Lévy flight gives an accurate physical description of radiation trapping [13] and enables precise experimental studies of light transport and Lévy parameters under tunable conditions [14].

Signatures of Lévy flights in atomic vapors were observed from the direct measurement of the step length distribution [9], the radial diffuse transmission [15, 16] and laser-frequency-dependent diffuse transmission [14, 17]. Time-resolved transmission was observed in the 1980s in sodium vapor for broad excitation [18] and data were analysed with transport radiative transfer equation [10, 11]. On the other hand, experiments with ultrashort laser pulses were performed in Lévy glasses [19], where the walk dimension was measured. In all these works, it was considered a slab geometry for the medium and the output photons were collected at the surface opposite to the laser input, i.e., photons in the forward direction or diffuse transmission.

In this work, we investigate the backward time-resolved scattered photons, i.e., the diffuse reflection, for photons in a hot atomic Rb vapor. We take advantage of a much higher number of detected photons, which implies a significantly higher signal-to-noise ratio (SNR). As a result, we achieved an SNR more than 50 times higher than that obtained from transmitted fluorescence measurements. We extract the Lévy parameter and clearly distinguish between single and multiple scattering, where the number of scattered photons is, respectively, small and large. For comparison, we also present results for the forward time-resolved transmission (diffuse transmission) and for the total diffuse transmission by scanning the incident laser detuning. Monte Carlo simulations confirm and support our experimental results. In addition, we show that at high density, diffuse transmission is com-

* michelle.oaraujo@ufpe.br

posed totally by multiple scattered photons, whereas for the diffuse reflection, an amount of 30% of the scattered photons have performed a single scattering event.

II. THEORY

We consider an atomic vapor at a temperature T and density $n = n(T)$. After a photon has been absorbed by an atom and emitted by spontaneous emission, it travels a distance x whose probability distribution is given by $P(x)$. The photon is emitted with a new frequency which depends on the incident frequency and the atom velocity. Assuming that the photon performs N_{sc} steps before leaving the vapor, for large N_{sc} we have complete frequency redistribution [20] and $P(x)$ is given by

$$P(x) = \int_{-\infty}^{\infty} k^2(\Delta) e^{-k(\Delta)x} d\Delta \xrightarrow{x \rightarrow \infty} \frac{1}{x^{\alpha+1}}, \quad (1)$$

where $\Delta = \omega - \omega_0$ is the photon detuning, with ω as the photon frequency and ω_0 as the atomic resonance frequency, $k(\Delta) = n\sigma_0 f(\Delta)$ is the absorption coefficient, n is the atom density and σ_0 is the resonant cross section. $f(\Delta)$ is the line shape, a Voigt profile given by

$$f(\Delta) \propto \frac{1}{\sqrt{\pi}u} \int_{-\infty}^{\infty} \frac{e^{-v^2/u^2}}{1 + 4(\Delta - kv)^2/\Gamma^2} dv. \quad (2)$$

In Eq. 2, v is the component of the atom velocity parallel to the photon, $u = \sqrt{2k_B T/M}$ is the most probable velocity, M is the atomic mass, T is the vapor temperature, k_B is the Boltzmann constant and Γ is the atomic natural linewidth. Eq. 2 takes into account the atom natural lineshape and the Doppler broadening. Approaching the Voigt profile core by a Doppler profile and from Eqs. 1 and 2, the parameter α , sometimes called Lévy index or Lévy exponent, is equal to $\alpha = 1$. For collisional broadening, Eq. 2 is replaced by a Lorentzian function with width $\Gamma_{col} \gg \Gamma$ and leads to Eq. 1 with $\alpha = 0.5$.

If the vapor cell has a slab geometry whose walls are at the positions $z = 0$ and $z = L$ along an z axis, and if photons enter at $z_0 \gtrsim 0$ ($0 < z_0 \ll L$), the temporal photon intensity profile at the forward exit surface ($z = L$) is called diffuse transmission. For large t , it is given by an exponential decay [15, 19, 21]

$$T_{\text{diff}}(t) \sim e^{-t/\tau}, \quad (3)$$

where [19]

$$\tau \propto L^d, \quad (4)$$

and d is called fractal dimension with $d = \alpha$ [21]. This

exponential decay was also reported in theories with radiative transport equation [10, 11], where the time decay rates were given as $\tau \propto b_0 \sqrt{\ln b_0} \propto b_0$ for Doppler broadening, where $b_0 = n\sigma_0 L$ is the resonant optical depth of the vapor.

On the other hand, the temporal intensity profile at the backward exit surface ($z = 0$) is called diffuse reflection, and for large t is given by [21]

$$R_{\text{diff}}(t) \sim e^{-t/\tau}, \quad (5)$$

i.e., the same exponential dependence as $T_{\text{diff}}(t)$. This suggests that it is possible to observe Lévy signatures from the backward transmission, and this is the aim of the present work. Also, a good signal-to-noise ratio is expected for photon collection in the backward direction, due to the so-called Ohm's law for photons [22, 23], i.e., $T_{\text{diff}} \rightarrow 0$ for large L for atoms in a slab geometry, which implies in increasing R_{diff} for large L . In this work, we replace L by the vapor density n in Eq. 4, since we keep L constant and vary n .

III. EXPERIMENT

A. Setup

Our experimental setup consists of a heated rubidium vapor cell, illuminated by a low-power homemade diode laser, resonant with the D2 line of rubidium ($\lambda = 780.24$ nm) and frequency stabilized by a saturated absorption setup (see Fig. 1). The laser beam is sent to a monomode PM optical fiber (not shown in Fig. 1). At the cell entrance, the laser beam is linearly polarized and has a diameter of 2 mm and 50 μ W power. The photodetectors PD1 and PD2 are detectors from ThorLabs, model APD120A/M, and collect the laser transmission (PD1; coherent transmission) and the emitted fluorescence (PD2) in the forward direction [diffuse transmission; Figs. 1(a) and (b)] or in the backward direction [Fig. 1(c)]. Both fluorescences are made of photons that performed a random walk in the vapor, and are collected by PD2 by means of a 30 mm focal lens, placed at a distance of approximately 10 cm from the oven aperture and at an angle of $\theta = 30^\circ$ from the laser direction. This angle is relatively large in order to minimize the scattered light by cell walls from coherent transmission. The cell is cylindrical where its main axis is placed perpendicularly to the laser beam direction. The cell has a length of 9 cm and a radius 1.25 cm. This cell setup was necessary because when directing the laser along the cell length, we observed a small diffuse transmission, i.e., practically no photons passing through the end. The cell is placed in a homemade oven that heats the entire unit. The oven has a circular aperture of diameter 2 cm (not shown in Fig. 1), from where the coherent transmission and the fluorescence exit.

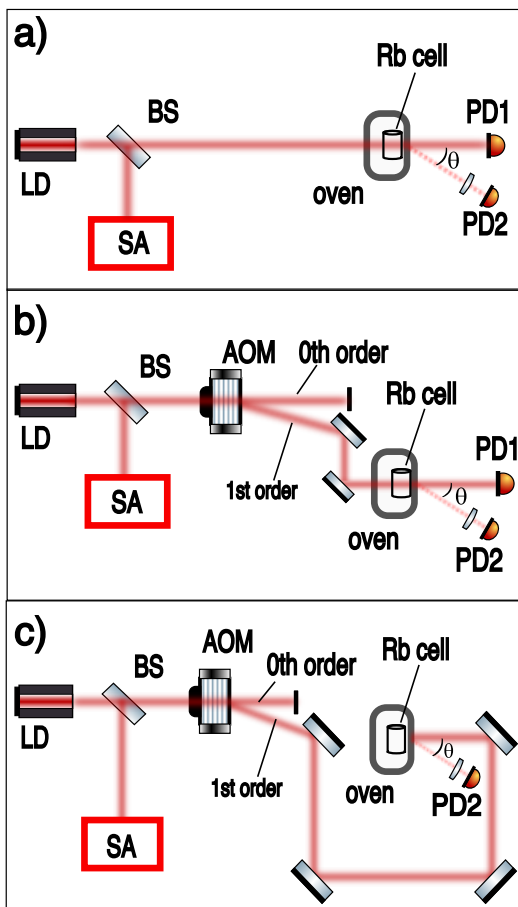


FIG. 1. (a) Scheme of the experimental setup. The laser diode (LD) is stabilized by a saturated-absorption spectroscopy (SA). The laser goes to a Rb cell in an oven. The photodetectors PD1 and PD2 measures, respectively, the coherent transmission and the diffuse transmission. (b) and (c) An AOM produces pulses. Its first-order beam (not shown) drives the vapor in order to measure the temporal diffuse transmission (b) or the diffuse reflection (c).

The laser coherent transmission as a function of the incident laser detuning Δ is theoretically adjusted in order to determine the vapor density n . For this, we adjust the coherent transmission (measured by photodetector PD1) with the Beer-Lambert law, $T_{\text{coh}}(\Delta) \propto e^{-n\sigma(\Delta)L}$, where the density n is kept as the free parameter and the cross section $\sigma(\Delta)$ takes into account the whole hyperfine structure of ^{85}Rb and ^{87}Rb . It is given by [24]

$$\sigma(\Delta) = \frac{\lambda^2}{2\pi} \left[\sum_{F=2}^3 \sum_{F'=1}^4 \frac{2F+1}{\sum_{F_1=2}^3 (2F_1+1)} \times \frac{S_{FF'}}{1+4(\omega-\omega_{FF'})^2/\Gamma^2} + \sum_{F=1}^2 \sum_{F'=0}^3 \frac{2F+1}{\sum_{F_1=1}^2 (2F_1+1)} \times \frac{S_{FF'}}{1+4(\omega-\omega_{FF'})^2/\Gamma^2} \right], \quad (6)$$

where $S_{FF'}$ are transition factors calculated from the Clebsch-Gordan and the Wigner 3- j coefficients [25] and $\omega_{FF'}$ is the transition frequency from the level F to F' . Temperatures range from 20°C to 145°C, which correspond to densities from 4.6×10^{15} to 4.2×10^{19} atoms/m³, respectively. Errorbars for the density were calculated for a set of few measurements with same temperature, and correspond to approximately 15% of its mean value.

In order to measure the temporal dynamics of the diffuse reflection and transmission, the laser has its frequency stabilized in the transition $F = 2 \rightarrow F' = 1, 2, 3$ of ^{87}Rb . The vapor is driven by square pulses of duration 16 μs , generated by the +1 order of an acousto-optical modulator (AOM) from Isomet, model 232A-1. The +1 order corresponds to 80 MHz above the transition $F = 2 \rightarrow F' = 3$ of ^{87}Rb . Note that due to the large Doppler broadening of the vapor, typically ~ 500 MHz, the exact value of the photon input frequency is not important, since it will be resonant with the vapor energy level or line inside this width. The AOM is placed at the focus of a telescope made of two lenses of focal distances 10 mm, in order to improve the pulse extinction time. Two detection schemes were employed: diffuse transmission [Fig. 1(b)] and diffuse reflection [Fig. 1(c)]. Each measured fluorescence for a fixed density is averaged for 2,000 cycles, corresponding to 2–3 hours of data acquisition.

To validate our experimental setup, we measure α using the method of ref. [14], done for a Cs vapor, which consists in scanning the incident laser frequency ω in order to measure the frequency-dependent diffuse transmission $T_{\text{diff}}(\Delta)$. Then we collect $T_{\text{diff}}(0)$, where $\Delta = 0$ corresponds to the transition $F = 2 \rightarrow F' = 3$ of ^{87}Rb , and plots it as a function of the vapor density n .

The diffuse transmission as a function of the detuning is shown in Fig. 2(a) for different temperatures when the laser is scanned around the transition $F = 2 \rightarrow F' = 1, 2, 3$ of ^{87}Rb D2 line. Note that $T_{\text{diff}}(0)$ is not equal to the minimum of $T_{\text{diff}}(\Delta)$ because the reference transition is close to the transition $F = 3 \rightarrow F' = 2, 3, 4$ of ^{85}Rb , so there is an overlap of wings of both Rb isotopes at $\Delta = 0$. Fig. 2(b) shows $T_{\text{diff}}(0)$ plotted as a function of the vapor density n , collected from $T = 70^\circ\text{C}$ ($n = 1.8 \times 10^{17}$ atoms/m³) to $T = 110^\circ\text{C}$ ($n = 3.3 \times 10^{18}$ atoms/m³). Between 30°C and 70°C and above 110°C,

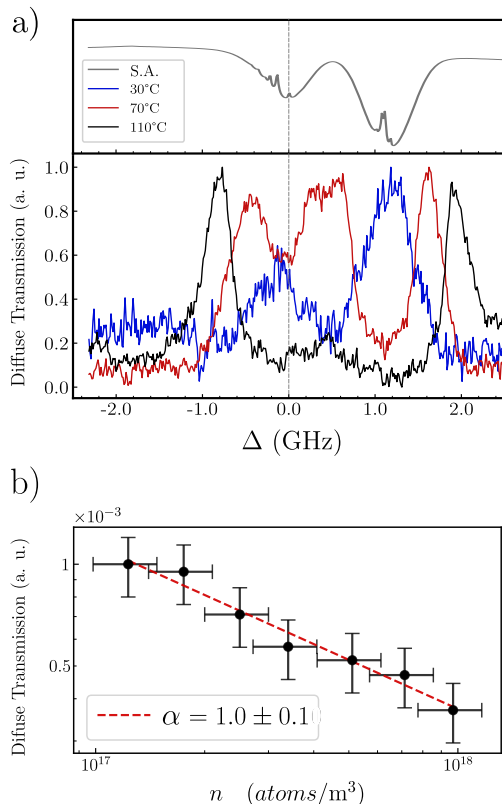


FIG. 2. (a) Diffuse transmission $T_{\text{diff}}(\Delta)$ as a function of the laser detuning for three different temperatures: 30°C (dark blue), 70°C (red) and 110°C (black). The top grey curve is the Rb saturated absorption (S.A.). (b) Measured diffuse transmission $T_{\text{diff}}(0)$ as a function of sample density n (black circles). The red dashed line is a fit of the experimental data with Eq. 7.

$T_{\text{diff}}(0)$ versus n is constant [not shown in Fig. 2(b)], due to low photon scattering number and detector noise level, respectively.

It was shown [14–16] that $T_{\text{diff}}(0)$ scales with n according to

$$T_{\text{diff}}(0) = \frac{C}{n^{\alpha/2}}, \quad (7)$$

where C is an arbitrary constant. We adjust our data with Eq. 7 by keeping C and α as free parameters. This gives $\alpha = 1.0 \pm 0.1$, i.e., consistent with $\alpha = 1$. Errorbars for $T_{\text{diff}}(0)$ were evaluated as the same way as those for n , i.e., by averaging a set of few measurements with same temperature and are approximately 20% of its mean value for a fixed n .

To investigate the possibility of collisions in our data, we estimate the atom-atom collisional rate as

$$\Gamma_{\text{col}} = \beta n, \quad (8)$$

where $\beta = 9 \times 10^{-8} \text{ Hz}\cdot\text{cm}^3$ [26]. For the range of densities in Fig. 2(b), this gives Γ_{col} between 15 kHz (for $n \approx 2 \times 10^{17} \text{ atoms/m}^3$) and 300 kHz (for $n \approx 3 \times 10^{18} \text{ atoms/m}^3$). Simulations were done from $T = 50^\circ\text{C}$ to $T = 130^\circ\text{C}$, which gives Γ_{col} between 4 kHz and 1 MHz (see details about the simulation methods in section IV). Also, we performed simulations by superestimating Eq. 8 by a factor of five and ten. Our simulations are in agreement with $\alpha = 1$. It is important to point out that ref. [14] reported a change from $\alpha = 1$ to $\alpha = 0.5$ for Cs vapor as n increases. Also, no collision effects were observed in the data of ref. [15], for a Rb vapor in a thin disk-shaped cell with densities up to $n = 1 \times 10^{20} \text{ atoms/m}^3$.

B. Experimental results

From the setup of Figs. 1(b) and (c), we extract, respectively, the temporal diffuse transmission $T_{\text{diff}}(t)$ and the temporal diffuse reflection $R_{\text{diff}}(t)$ as a function of the time t , for a given density n . Typical curves are shown in Figs. 3(a) and 4(a). The curves were normalized by their mean value in the range $t/\tau_0 \in [-12, -9]$ (i.e., before the AOM switch off) and correspond to ≈ 200 points. The time t is normalized by the Rb natural time decay rate $\tau_0 = 1/\Gamma \approx 26 \text{ ns}$. At the lowest temperature, $T = 20^\circ\text{C}$ [density $n = 4.6 \times 10^{15} \text{ atoms/m}^3$; not shown in Fig. 2(a)], density is not high enough and the decay is approximately equal to the laser switch off extinction generated by the AOM, which is 16 ns. For all temperatures, we identify an exponential decay in the range $I(t) \in [0.3, 0.8]$, where $I(t) = \{T_{\text{diff}}(t), R_{\text{diff}}(t)\}$.

For $T_{\text{diff}}(t)$, data were acquired from $T = 24^\circ\text{C}$ ($n = 6.1 \times 10^{15} \text{ atoms/m}^3$) to $T = 80^\circ\text{C}$ ($n = 3.6 \times 10^{17} \text{ atoms/m}^3$). For higher temperatures, few photons are collected and we have a bad signal-to-noise ratio, and consequently no data in the mentioned range. On the other hand, for $R_{\text{diff}}(t)$, we have achieved temperatures of $T = 145^\circ\text{C}$ ($n = 4.2 \times 10^{19} \text{ atoms/m}^3$). Also, we checked that $R_{\text{diff}}(t)$ curves saturate and collapse from $T > 115^\circ\text{C}$ ($n > 4.7 \times 10^{18} \text{ atoms/m}^3$) [not shown in Fig. 4(a)]. Note that the total amount of forward diffuse photons, given by Eq. 7 for a slab geometry [15], tend to zero for large n , which means that the total amount of backward diffuse photons tend to the input photon number.

The temporal decay rate of these curves were extracted by using an exponential function $I(t) = Ae^{-t/\tau}$ [15, 19, 21], where A and τ were kept as free parameters. Then, we plot τ versus the density n . A theoretical fitting is done using a power-law equation [21]:

$$\tau = Bn^\alpha, \quad (9)$$

where B and α were kept as free parameters.

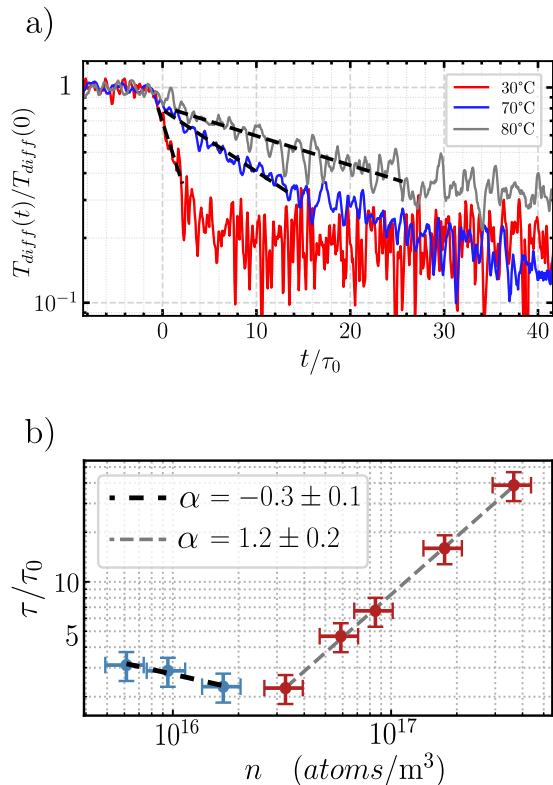


FIG. 3. (a) Normalized temporal diffuse transmission $T_{\text{diff}}(t)$ as a function of the normalized time t/τ_0 for three different temperatures: 30°C (red), 70°C (blue) and 80°C (gray). The dashed black lines are the respective theoretical fitting curves in the interval $I(t)/I_0 \in [0.3, 0.8]$. (b) Decay times τ/τ_0 as a function of the density n from $T_{\text{diff}}(t)$ shown in panel (a). The different colors separate low and high densities. The dashed lines are the respective theoretical adjusts using Eq. 9.

The experimental data for τ and the corresponding fitting curves are given in Figs. 3(b) and 4(b) for the diffuse transmission and reflection, respectively. We see two dominant regions: for low density, we have $\alpha \approx 0$, i.e., a constant region, whereas for high densities α is close to unity. We extract $\alpha = 1.2 \pm 0.2$ for the transmission data and $\alpha = 0.9 \pm 0.1$ for the reflection data, which is in agreement with the expected $\alpha = 1$ and confirms that there are signatures of Lévy flights from the backward fluorescence. This is the main result of this work. Note that these data are also in agreement with the frequency-dependent diffuse transmission (Fig. 2). We also checked that our data is consistent with the predictions from radiative transport equation [10], namely, $\tau/\tau_0 \propto n\sqrt{\ln n} \approx n$ for large n .

IV. SIMULATIONS

The observation of Lévy statistics from the backward fluorescence (Fig. 4), discussed in the last section, is due to the Lévy flights of backward photons and it is in agree-

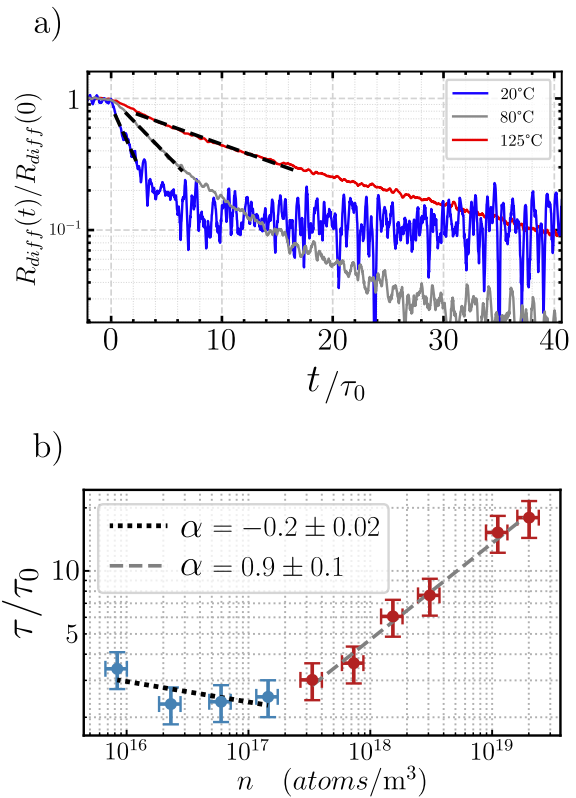


FIG. 4. (a) Normalized temporal diffuse reflection $R_{\text{diff}}(t)$ as a function of the normalized time t/τ_0 for three different temperatures: 20°C (blue; $n = 4.6 \times 10^{15}$ atoms/m³), 80°C (gray; $n = 3.7 \times 10^{17}$ atoms/m³) and 125°C (red; $n = 9.7 \times 10^{18}$ atoms/m³). The dashed black lines are the respective theoretical fitting curves in the interval $R_{\text{diff}}(t)/R_0 \in [0.3, 0.8]$. (b) Decay times τ/τ_0 as a function of the density n from $R_{\text{diff}}(t)$ shown in panel (a). The different colors separate low and high densities. The dashed lines are the respective theoretical adjusts using a power law function.

ment with the observed data from the forward fluorescence, for both temporal dynamics (Fig. 3) and steady frequency-dependent (Fig. 2). However, for low densities [blue dots in Figs. 3(b) and 4(b)], the observed data are not compatible with a Lévy statistics. At the same time, for high n , since the photon has its first absorption close to the input cell window and due to the spatial isotropy of spontaneous emission, it may be backward scattered and leave the vapor after a single scattering event.

To address these and other questions, we perform Monte Carlo simulations to compare with our data. The simulations methods are discussed elsewhere [28]. In simplified words, we send a number N_{ph} of photons with detuning $\Delta = 0$ into a vapor with density n and temperature T . For each photon, we draw the step length x the photon walks before finding a two-level atom. The probability distribution of x for a given detuning is $P_{\Delta}(x) = e^{-k(\Delta)x}$, where $k(\Delta)$ is the vapor absorption coefficient given by $k(\Delta) = n\sigma_0 f(\Delta)$ and Eq. 2. After finding an atom, we draw the scattering direction

of the photon and calculate its new Δ , where Δ is re-distributed by Doppler effect and depends on the atom velocity components, which are drawn from a Maxwell-Boltzmann distribution with temperature T . Then, we draw x from $P_{\Delta}(x)$ for this new detuning, and we repeat the steps until the photon leaves the cell. The cell is modelled as in the experiment, with same dimensions and orientation (see subsection III A). After the photon leaves the cell, we save its number of scattering events N_{sc} and its output detuning Δ .

The method described above does not take into account atomic collisions. To simulate collisional effects, we replace Γ in Eq. 2 by $\Gamma_{tot} = \Gamma + \Gamma_{col}$, where Γ_{col} is the collisional rate, given by Eq. 8. Then we define the collision probability as $P_{col} = \Gamma_{col}/(\Gamma + \Gamma_{col})$ [14], and we draw a number between 0 and 1 to compare with P_{col} . If a collision does not occur, we calculate the new detuning Δ as before. If a collision occurs, we draw the new photon detuning Δ from a Lorentzian distribution of width Γ_{col} and then we correct it by Doppler effect only in the emission.

A. Increase of the scattered photons in the backward direction

The total number N_{sc} of scattered photons (no matter their output detuning and how many steps they performed before leaving the vapor) can be collected in the forward region (between 0° and 90° from the incidence direction) or in the backward direction (from 90° to 180° from the incidence direction). These quantities are the total diffuse transmission and reflection, respectively. For our experimental data, they correspond to the steady values of the temporal diffuse and reflection, i.e., before the laser pulse is extinguished.

Figure 5 displays the total transmission and reflection as a function of the density n , as well as the experimental data for the diffuse reflection for comparison. The experimental data are the average value of the diffuse reflection $R_{diff}(t)$ in the time range $t/\tau_0 \in [-12, -9]$. We see [Fig. 5(a)] that R_{diff} saturates, and our experimental data [Fig. 5(b)] follows the same behavior. Meanwhile, T_{diff} tends to zero. A theoretical adjust from the third value of n with Eq. 7 [not shown in Fig. 5(a)] gives $\alpha = 1.07 \pm 0.07$, consistent with Lévy flights. This is to be compared with the so-called Ohm's law for photon scattering [22], observed in cold atoms [23, 27], where the diffuse transmission decays with $1/n$.

B. Single and multiple scattering in the decay dynamics

In order to simulate the temporal emitted fluorescences, named diffuse transmission and diffuse reflection, we assume that the N_{ph} photons enter at the cell at the same time, and thus we obtain a histogram of the number

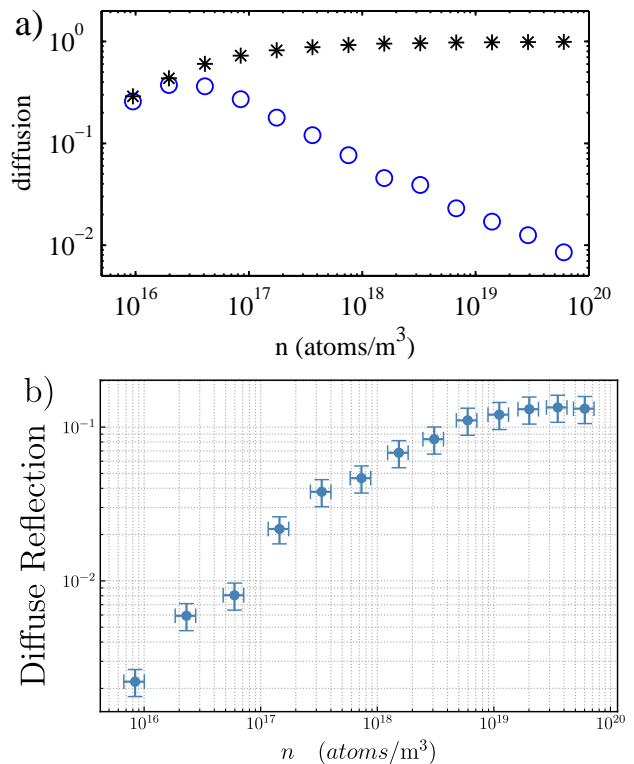


FIG. 5. (a) Steady diffuse transmission (blue circles) and reflection (black asterisks) from simulations as a function of the vapor density. The vertical axis is normalized by the total amount of input photons, which is 2,000. (b) Experimental diffuse reflection in arbitrary units in the steady state as a function of density.

of exiting photons as a function of N_{sc} . Note that the time the photon spent in the vapor is given by $\tau = N_{sc}\tau_0$, since the travel time between two scattering events is negligible. To simulate the effect of a square pulse of duration Δt_p driving the vapor, we make a convolution of the obtained histogram and a square pulse [29]. Then, we normalize its maximum value to unity.

Figure 6(a) compares directly the normalized temporal diffuse transmission and reflection, for several temperatures. At low temperatures (i.e., low n), both curves are similar with a single predominant exponential decay. However, at high temperatures (i.e., high n), whereas a single exponential decay is present for diffuse transmission, two exponential decays are present in diffuse reflection: a fast decay, for $I(t)/I(0) > 10^{-1}$, and a late exponential decay, for $I(t)/I(0) < 10^{-1}$. We adjust these decays with an exponential law in each time range in order to extract the time decay rates.

The time decay rates are plotted in Fig. 6(b). For $T_{diff}(t)$, the fit range is $I(t) \in [0.01, 0.9]$. A fit with Eq. 9 leads to $\alpha = 0.92 \pm 0.05$. For $R_{diff}(t)$, τ extracted in the early-time interval $I(t)/I(0) \in [0.2, 0.8]$ gives $\alpha \approx 0.5$ [not shown in Fig. 6(b)], whereas τ extracted from the

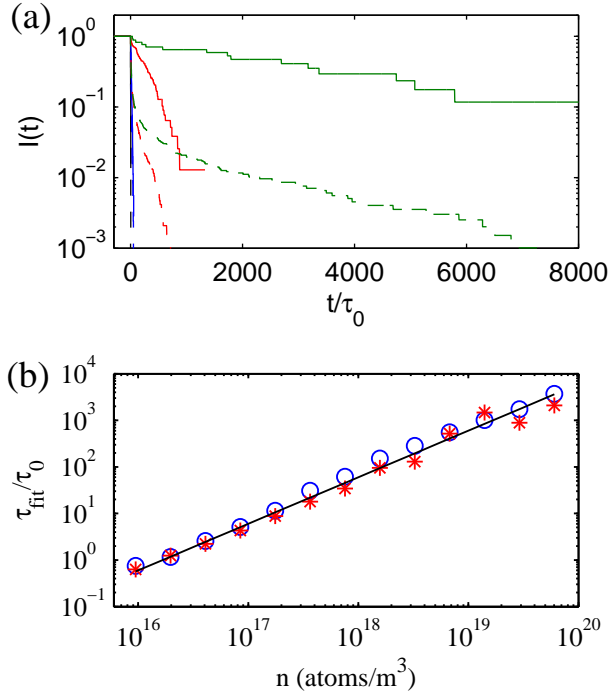


FIG. 6. (a) Normalized temporal fluorescences as a function of the time for 30°C (black; $n = 9.5 \times 10^{15}$ atoms/m³), 70°C (blue; $n = 1.8 \times 10^{17}$ atoms/m³), 110°C (red; $n = 3.3 \times 10^{18}$ atoms/m³) and 150°C (green; $n = 6.0 \times 10^{19}$ atoms/m³). Full lines (dashed lines) are for diffuse transmission (diffuse reflection). (b) Normalized decay times τ/τ_0 as a function of the density n from the temporal diffuse transmission (blue circles) and diffuse reflection (red asterisks). The full black line is the theoretical curve $\tau/\tau_0 \propto n^\alpha$ with $\alpha = 1$.

late time region $I(t)/I(0) \in [0.01, 0.1]$ gives $\alpha = 0.8 \pm 0.2$. For comparison, a curve $\tau \propto n^1$ is also shown. We find total agreement with our experiment. Note that the simulations were performed with two-level atoms, and due to this we do not expect quantitative agreement.

C. Presence of single scattering in diffuse reflection for high density

At low density n , many photons leave the vapor with low scattering event number, typically $N_{sc} = 1$, both for diffuse transmission and reflection. As n increases, the typical step length ℓ between two scattering events, given by $\ell = 1/[n\sigma_0 f(0)]$, decreases, so more photons perform more scattering events before leaving the vapor. Also, the distance z_0 travelled by the photon between the cell input wall and the first scattering event is of order of $z_0 \sim \ell$. This number becomes close to μm for high densities, which means that for diffuse reflection, there is a significant amount of photons which are scattered with low N_{sc} , since the first scattering event occur close to the

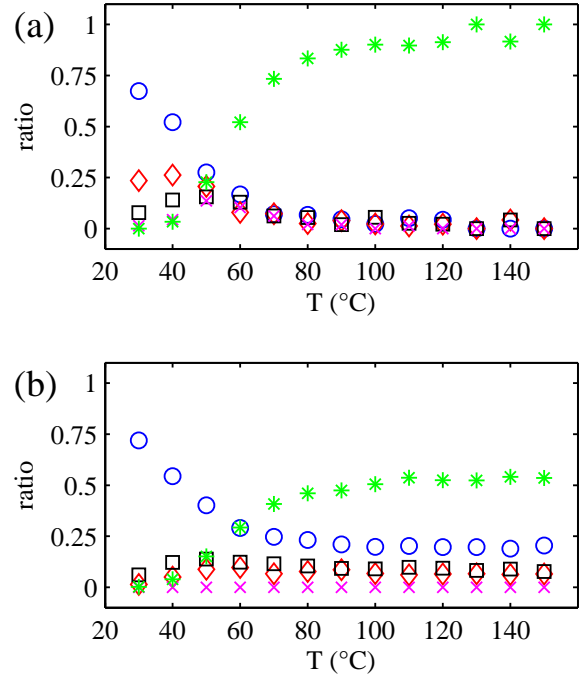


FIG. 7. Ratio between the amount of scattered photons (ratio S.S.) for a fixed N_{sc} and the total amount of scattered photons for a fixed temperature, for (a) diffuse transmission and (b) diffused reflection. Legend: $N_{sc} = 1$ (blue \circ), $N_{sc} = 1$ (red \diamond), $N_{sc} = 3$ (black \square), $N_{sc} = 4$ (magenta \times) and $N_{sc} \geq 5$ (green $*$).

cell wall and the scattering is isotropic.

We quantify the number of scattering events performed by the photons both for diffuse transmission and reflection after they left the vapor. Fig. 7 displays the results. The vertical axis is the number of photons which left the vapor with a given N_{sc} in a given direction (transmission or reflection) divided by the total amount of photons scattered in the same direction, for a fixed temperature. Temperatures go from 30°C to 150°C, which implies in densities from $n = 9.5 \times 10^{15}$ to $n = 6.0 \times 10^{19}$ atoms/m³, respectively. For diffuse transmission [Fig. 7(a)], the amount of photons which performed low scattering events ($N_{sc} \leq 4$) decreases quickly for increasing temperature T , becoming zero for $T \geq 100^\circ\text{C}$ ($n \geq 1.6 \times 10^{18}$ atoms/m³). This means that in this range almost all photons (0.9, i.e., 90%) leave the vapor performing $N_{sc} \geq 5$ scattering events. This means multiple scattering, complete frequency redistribution and consequently a single decay for $T_{\text{diff}}(t)$, observed in both experimental and theoretical results. On the other hand, for the photons emitted backward [Fig. 7(b)], the amount of single scattered photons ($N_{sc} = 1$) tends to a steady value of 0.20 (i.e., 20%) for $T \geq 100^\circ\text{C}$. For $N_{sc} = 2$ and $N_{sc} = 3$, we have, respectively, a fraction of 0.09 and 0.06. This means that $\sim 35\%$ of the diffuse reflected photons have performed

few scattering events before leaving the medium, even for high density, which would imply in partial frequency redistribution and a Lévy parameter of $\alpha > 1$ [30]. On the other hand, the fraction of scattered photons with $N_{sc} \geq 5$ is approximately 0.50, i.e., 50%. However, we still see $\alpha = 1$ in the temporal dynamics, meaning that these $\sim 50\%$ of photons dominate the statistics of the emitted fluorescence in the backward direction for large times and lead to the observation of $\alpha = 1$.

V. CONCLUSIONS

We have studied the temporal dynamics of Lévy flights in a hot rubidium vapor as a function of its density, and we have shown that it is possible to see Lévy signatures from the fluorescence emitted backward (diffuse reflection). We observed in this regime the Lévy parameter $\alpha = 1$, which is consistent with the forward emitted fluorescence (diffuse transmission) in the temporal regime and in the stationary regime. Monte Carlo simulations confirm our findings. All simulations were done for two-level atoms, where the results are found to be consistent with previous experiments [24]. The impact of the atomic multilevel structure was studied recently [31].

For increasing density vapor, the photons tend to be scattered backward, which represents a significant improvement of signal-to-noise ratio compared to diffuse transmission. However, we have a significant amount of photons emitted after few scattering events, specially single scattering, in contrast with the forward fluorescence where almost all photons have performed multiple steps.

It is surprising that a collected fluorescence is composed of half of photons performing a single scattering event and the few multiple scattered photons dominate the observed value of α .

This work is a first investigation of the Lévy parameter via backscattered light. Extensions of this work include the short excitation regime, where the excitation duration is smaller than the atomic lifetime and would imply in different behavior of the photons during the random walk with respect to their time scales. In this context, normal diffusion has been observed in biological tissue [5] and Lévy diffusion in Lévy glasses [19]. We hope this work can contribute to further investigations of photon diffusion.

ACKNOWLEDGEMENTS

We thank Sandra S. Vianna for borrowing the cell oven and detectors, and Naudson L. L. Matias and Nicolas A. Pessoa for helping on the experimental setup and data analysis, respectively. We also acknowledge the financial support from UFPB, UFPE and the agencies Army Research Office (Grant No. W911NF-23-1-0287), Coordenação de Aperfeiçoamento de Pessoal de Nível Superior (CAPES), Conselho Nacional de Desenvolvimento Científico e Tecnológico (CNPq), Fundação de Amparo à Ciência do Estado de Pernambuco (FACEPE), FAPESP (2021/06535-0), National Quantum Information Institute (INCT-IQ, No. 410 465469/2014-0)/CNPq, and the National Photonics Institute (INCT-INFo, No. 409174/2024-6)/CNPq.

-
- [1] G. M. Viswanathan, V. Afanasyev, S. V. Buldyrev, E. J. Murphy, P. A. Prince, and H. E. Stanley, *Nature* **381**, 413 (1996).
 - [2] A. M. Edwards, R. A. Phillips, N. W. Watkins, M. P. Freeman, E. J. Murphy, V. Afanasyev, S. V. Buldyrev, M. G. E. da Luz, E. P. Raposo, H. E. Stanley, and G. M. Viswanathan, *Nature* **449**, 1044 (2007).
 - [3] J. Li, L. Weng, J. Xie, J. Amrit, and A. Ramiere, *Physical Review E* **105**, 064123 (2022).
 - [4] T. B. Smith and D. B. Weissman, G3: Genes, Genomes, Genetics **13**, jkad023 (2023).
 - [5] V. V. Chernomordik, D. W. Hattery, D. Grosenick, H. Wabnitz, H. H. Rinneberg, K. T. Moesta, P. M. Schlag, and A. H. Gandjbakhche, *Journal of Biomedical Optics* **7**, 80 (2002).
 - [6] G. Labeyrie, E. Vaujour, C. A. Müller, D. Delande, C. Miniatura, D. Wilkowski, and R. Kaiser, *Physical Review Letters* **91**, 223904 (2003).
 - [7] V. V. Ivanov and J. M. Dlugach, *Journal of Quantitative Spectroscopy and Radiative Transfer* **323**, 108999 (2024).
 - [8] P. Barthelemy, J. Bertolotti, and D. S. Wiersma, *Nature* **453**, 495 (2008).
 - [9] N. Mercadier, W. Guerin, M. Chevrollier, and R. Kaiser, *Nature Physics* **5**, 602 (2009).
 - [10] T. Holstein, *Physical Review* **72**, 1212 (1947).
 - [11] T. Holstein, *Physical Review* **83**, 1159 (1951).
 - [12] A. R. Alves-Pereira, E. J. Nunes-Pereira, J. M. G. Martinho, and M. N. Berberan-Santos, *The Journal of Chemical Physics* **126**, 154505 (2007).
 - [13] M. Chevrollier, *Contemporary Physics* **53**, 227 (2012).
 - [14] A. S. M. Macedo, J. P. Lopez, and T. Passerat de Silans, *Physical Review E* **104**, 054143 (2021).
 - [15] Q. Baudouin, R. Pierrat, A. Eloy, E. J. Nunes-Pereira, P.-A. Cuniasse, N. Mercadier, and R. Kaiser, *Physical Review E* **90**, 052114 (2014).
 - [16] M. O. Araújo, T. P. de Silans, and R. Kaiser, *Physical Review E* **103**, L010101 (2021).
 - [17] J. P. Lopez, A. S. M. Macedo, M. O. Araújo, and T. Passerat de Silans, *Physical Review A* **107**, 013501 (2023).
 - [18] T. Colbert and J. Huennekens, *Physical Review A* **41**, 6145 (1990).
 - [19] R. Savo, M. Burreli, T. Svensson, K. Vynck, and D. S. Wiersma, *Physical Review A* **90**, 023839 (2014).
 - [20] E. Pereira, J. M. G. Martinho, and M. N. Berberan-Santos, *Physical Review Letters* **93**, 120201 (2004).
 - [21] J. Klinger, R. Voituriez, and O. Bénichou, *Physical Review E* **107**, 054109 (2023).

- [22] M. C. W. van Rossum and T. M. Nieuwenhuizen, *Review of Modern Physics* **71**, 313 (1999).
- [23] W. Guerin, M. Rouabah, and R. Kaiser, *Journal of Modern Optics* **64**, 895 (2017).
- [24] N. Mercadier, M. Chevrollier, W. Guerin, and R. Kaiser, *Physical Review A* **87**, 063837 (2013).
- [25] D. A. Steck, Rubidium D Line Data, <http://steck.us/alkalidata>, 2025.
- [26] L. Weller, R. J. Bettles, P. Siddons, C. S. Adams, and I. G. Hughes, *Journal of Physics B: Atomic, Molecular and Optical Physics* **44**, 195006 (2011).
- [27] G. Labeyrie, D. Delande, C. Müller, C. Miniatura, and R. Kaiser, *Optics Communications* **243**, 157 (2004).
- [28] J. C. de A. Carvalho, M. Oriá, M. Chevrollier, H. L. D. de S. Cavalcante, and T. Passerat de Silans, *Physical Review A* **91**, 053846 (2015).
- [29] G. Labeyrie, R. Kaiser, and D. Delande, *Applied Physics B* **81**, 1001 (2005).
- [30] M. Chevrollier, N. Mercadier, W. Guerin, and R. Kaiser, *The European Physical Journal D* **58**, 161 (2010).
- [31] I. C. Nunes, M. O. Araújo, J. P. Lopez, and T. Passerat de Silans, *Journal of Quantitative Spectroscopy and Radiative Transfer* **343**, 109481 (2025).